Contactless measurements of Shubnikov-de Haas oscillations in the magnetically ordered state of CeAgSb$_2$ and SmAgSb$_2$ single crystals

Ruslan Prozorov,[*] Matthew D. Vannette, German D. Samolyuk, Stephanie A. Law, Sergey L. Bud'ko, and Paul C. Canfield

Ames Laboratory and Department of Physics and Astronomy, Iowa State University, Ames, Iowa 50011, USA

Shubnikov-de Haas oscillations were measured in single crystals of highly metallic antiferromagnetic SmAgSb$_2$ and ferromagnetic CeAgSb$_2$ using a tunnel diode resonator. Resistivity oscillations as a function of applied magnetic field were observed via measurements of skin depth variation. The effective resolution of $\Delta\rho \simeq 20$ pΩ allows a detailed study of the SdH spectra as a function of temperature. The effects of the Sm long-range magnetic ordering as well as its electronic structure (4f electrons) on the Fermi surface topology is discussed.

I. INTRODUCTION

Measurements of quantum oscillations in the resistivity [Shubnikov-de Haas effect (SdH)] and in the magnetization [de Haas-van Alphen effect (dHvA)] are among the primary experimental techniques to study the geometry of Fermi surfaces in metals.[1,2] Although both originate from the basic physics of Landau quantization of electron orbits in a magnetic field, the coupling of electron motion to resistivity is different from that of magnetization. Electron transport depends on the density of states and the scattering rates, both modulated by the Landau quantization. Within a standard theory[1] for a three-dimensional Fermi surface the amplitude of the rth harmonic oscillatory part of magnetization is given by (Ref. [2]),

$$M_r \propto \frac{S_{extr} B^{1/2}}{m_c |S''|_{extr}^{1/2}} R_T(r) R_D(r) R_S(r), \quad (1)$$

where m_c is the cyclotron mass, S_{extr} is the extremal cross section of the Fermi surface (FS), $|S''|_{extr} = (\partial^2 S / \partial p_B^2)_{extr}$ is a measure of the FS curvature along **B** at the extremal cross section, and the damping factors R_T, R_D, and R_S are caused by finite temperature, scattering, and Zeeman splitting, respectively. The corresponding fundamental frequency is

$$f = \frac{S_{extr}}{he}. \quad (2)$$

On the other hand, the amplitude of Shubnikov-de Haas oscillations in electrical resistivity (when the oscillatory component is much smaller than the background) is proportional to

$$\alpha_r \propto \frac{m_c S_{extr} B^{1/2}}{|S''|_{extr}^{1/2}} R_T(r) R_D(r) R_S(r) \quad (3)$$

with the same damping factors as for dHvA effect. Resistivity oscillations in three-dimensional (3D) metals are generally more difficult to measure, especially in highly conducting samples. The problem is worse for small single crystals where attaching the contacts is not an easy task. It should be noted that the SdH amplitude dependence on the m_c is reciprocal to the dHvA amplitudes: $\alpha_r / M_r \propto m_c^2$, so for small m_c, the relative amplitude of the SdH oscillations is decreased.

The alternative to direct transport measurements is to measure the skin depth. This paper describes the use of highly sensitive tunnel-diode oscillator technique for the quantitative study of quantum oscillations in metallic samples. The technique is especially useful for small samples when attachment of contacts is difficult. Detailed analysis of the raw data is presented.

II. THE TECHNIQUE

An oscillating magnetic field of frequency f penetrates a metallic sample, decaying in a typical length δ, the skin depth. In the local limit, where $E = \rho j$, δ is given by the normal skin effect expression (Ref. [3]),

$$\delta = \frac{c}{2\pi} \sqrt{\frac{\rho}{\mu f}}, \quad (4)$$

where ρ is resistivity and μ is magnetic permeability. Unfortunately, typical AC magnetometers are not sensitive enough to measure this depth with sufficient precision. In addition, for typical low-frequency magnetometers (up to kHz frequencies), skin depth is too large compared to the small crystal size. For higher-frequency techniques, such as microwave or infrared reflectivity and absorption, the anomalous skin effect and possible dynamic effects (e.g., magnetic relaxation) take place. Although the anomalous skin effect was originally used to study Fermi surfaces,[4] in the extreme anomalous limit the skin effect is no longer determined only by the resistivity, but also by the electronic mean free path, ℓ. The skin depth then depends on a product $\rho\ell$, which is independent of the scattering rate and cannot be used for contactless measurements of resistivity.

In this work, a self-resonating, tunnel diode driven LC circuit was used for precise measurements of the effect of temperature and magnetic field on the skin depth of CeAgSb$_2$ and SmAgSb$_2$. The circuit had a natural oscillation frequency of $\simeq 10$ MHz. Originally, this technique was developed to measure London penetration depth in small superconducting crystals, where its great sensitivity was a key factor. Details of the apparatus and calibration are given elsewhere.[5,6] Tunnel diode resonators have been used for qualitative studies of the skin depth oscillations in pulsed

magnetic fields in organic superconductors with relatively large normal-state resistivities ($>200\ \mu\Omega$ cm).[7,8] Although little quantitative analysis was reported, these studies demonstrate the effectiveness of the technique.

When a metallic sample is inserted into a coil which is part of an LC circuit the resonant frequency changes from f_0 to f. This change is caused by two effects: the diamagnetic skin effect, which screens the alternating magnetic field from the bulk of the sample and the magnetic permeability μ of the sample. The measured frequency shift $\Delta f = f(T, H) - f_0$ is given by the total dynamic magnetic susceptibility of the sample, $\chi = dM/dH$ (Ref. 5),

$$\frac{\Delta f}{\Delta f_0} = 1 - \frac{\mu\delta}{2R} \tanh\left(\frac{2R}{\mu\delta}\right), \tag{5}$$

where R is the effective sample dimension (for an infinite slab of width w, $R = w/2$) and skin depth δ is given by Eq. (4). The maximal expulsion frequency, Δf_0, (frequency shift in the limit of a perfect conductor with $\delta = 0$) depends only on the geometry of the sample and parameters of empty resonator and is given by

$$\Delta f_0 = \frac{fV}{2V_0(1 - N)}, \tag{6}$$

where V is the sample volume, V_0 is the effective coil volume, and N is the demagnetization factor.[5] In deriving Eq. (5) it is assumed that $\Delta f_0 \ll f_0$, which is always the case in our frequency and sample size range (the base frequency is approximately $f_0 = 10^7$ Hz, whereas typical $\Delta f_0 = 10^4$ Hz). The factor μ in Eq. (5) comes from the direct magnetic contribution of magnetic permeability in the skin layer via $B = \mu H$, which enters the total magnetic moment after integration over the sample volume. A similar effect was discussed before for superconductors.[9] However, the direct contribution of magnetic permeability in the samples under study is minor. This is because we obtain useful information only well below the ordering temperature and in high magnetic fields where $\mu \approx 1$. The oscillating part of the permeability is small due to very small excitation field, $H_{ac} \approx 20$ mOe. In addition, magnetic field only penetrates the skin depth layer and its direct contribution to the total susceptibility is attenuated by the factor of (δ/R) compared to the skin effect contribution. In other magnetic systems with large polarizability or in the vicinity of the magnetic ordering temperature, direct magnetic contribution could be important, but this is not relevant to the present work.

Obviously, the described technique is sensitive only as long as the skin depth is less than the effective sample size. For larger skin depth (larger resistivity), the sample becomes transparent to an oscillating magnetic field. For example, in our particular setup in actual units,

$$\delta[\mu m] = 15\sqrt{\rho[\mu\Omega\ cm]}. \tag{7}$$

With small crystals of typical size of $R = 500\ \mu$m, we can roughly estimate the upper limit where the described technique is sensitive. By equating $\delta_{max} = R$, we obtain $\rho_{max} = (500/15)^2 \approx 1000\ \mu\Omega$ cm. Measurements on samples with larger resistivities are possible, but require larger samples or

higher frequencies (both of which are possible). At the opposite extreme for samples with very small resistivities, the limitation is the anomalous skin effect, which becomes relevant when skin depth becomes smaller than the electronic mean free path, ℓ, and the local version of the Ohm's law is no longer valid. We can roughly estimate the lower threshold of resistivity below which anomalous skin effect takes place by using a Drude approximation for which the mean free path is given by

$$\ell = \frac{(3\pi^2)^{1/3}\hbar}{n^{2/3}e^2\rho}, \tag{8}$$

where n is the electron density and e is the electron charge. Therefore, using Eq. (4) we obtain ρ_{min} at which $\ell = \delta$,

$$\rho_{min} = \left(\frac{\mu f\pi^{7/3}3^{2/3}\hbar^2}{n^{4/3}e^4}\right)^{1/3} \approx 8.6 \times \frac{(\mu f)^{1/3}}{n^{4/9}}. \tag{9}$$

For a typical nonmagnetic metal with $n = 5 \times 10^{28}$ m^{-3} and our frequency, $f = 10^7$ Hz, we obtain $\rho_{min} \approx 0.03\ \mu\Omega$ cm. Therefore, our method allows direct quantitative study of (contactless) resistivity in small crystals approximately in the range of $0.03 - 1000\ \mu\Omega$ cm, which covers most metallic materials of interest. Furthermore, the difficulty of measuring small highly conducting samples by conventional means turns to be an advantage for the data analysis. In the regime of good metals, the data is significantly simplified, because the $\tanh(R/\delta)$ term in Eq. (5) becomes relevant only for $\delta \gtrsim 0.2R$. In the samples discussed below, the resistivity varies between $0.1 - 10\ \mu\Omega$ cm, for which $\delta/R = 0.01 - 0.1$ and therefore, we can simply use the linear version of Eq. (5),

$$\frac{\Delta f}{\Delta f_0} = 1 - \frac{\mu\delta}{2R}. \tag{10}$$

It should be noted that it is still straightforward to invert full Eq. (5) to obtain the skin depth numerically.

In the measurements reported below, slab-shaped samples were positioned inside the resonant coil on a sapphire sample holder. The crystallographic c axis was parallel to both the AC excitation and DC magnetic fields. In this arrangement, screening currents flowed in the ab plane and therefore the in-plane component of the resistivity was measured. A typical run was from 0 to 90 kOe DC field and back to 0 with about 10 000 data points taken in each leg. Various ramp rates where used with the slowest being 3.5 Oe/s.

III. SAMPLES

In this work, the skin depth was measured in two isostructural tetragonal intermetallic compounds: $CeAgSb_2$ and $SmAgSb_2$ single crystals. Both materials (and related compounds) were studied before,[10–14] though with much more attention to $CeAgSb_2$ which undergoes a ferromagnetic transition along the c axis below $T_c = 9.8$ K. $SmAgSb_2$ is antiferromagnetic with $T_N = 9.5$ K. Transport and magnetic properties, including direct measurements of dHvA and SdH effects were reported previously.[12–14] Whereas SdH in $CeAgSb_2$ showed a single dominant frequency at 0.25 MG, in $SmAgSb_2$ the behavior is much more complex with several
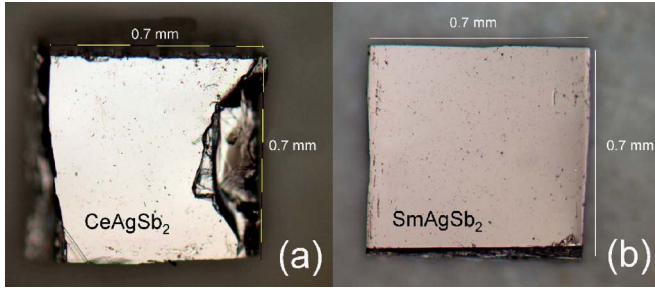
FIG. 1. (Color online) Optical images of studied crystals. (a) $CeAgSb_2$ and (b) $SmAgSb_2$. Each crystal was $0.7 \times 0.7 \times 0.3$ mm^3.

frequencies and significant difference between dHvA and SdH spectra. One difference between $CeAgSb_2$ and $SmAgSb_2$ is substantially larger scattering rates in the former (as evident from *RRR*). Also, as we show below, small changes in the Fermi level lead to significant changes of the Fermi surface structure and appearance of new extremal orbits.

Single crystals of $CeAgSb_2$ and $SmAgSb_2$ were grown out of Sb flux.[12,15] The starting materials were placed in an alumina crucible and sealed under vacuum in a quartz ampule, heated to 1150 °C, and then cooled to 670 °C over 120 h. The best crystals with the cleanest surface were selected and cut with a blade along the sides for the measurements. The samples are shown in Fig. 1. The c axis was perpendicular to the largest face. The residual resistivity ratio, $RRR = \rho(300 \text{ K})/\rho(2 \text{ K})$ was determined by standard four-point measurements. For $SmAgSb_2$ we obtained $RRR = 200$ and for $CeAgSb_2$ $RRR = 70$. The transport measurements were performed on bar-shaped samples from the same batches that were used for resonator measurements, shown in Fig. 1.

IV. RESULTS

Figure 2 shows resistivity versus temperature obtained from the frequency shift by using Eqs. (5) and (4). The skin depth is shown in the inset. The high-temperature (at $T=20$ K) resistivity data was used to normalize the calibration constant, Δf_0. Direct calibration with known parameters of the oscillator produce very similar temperature dependence, but the offset (residual resistivity) cannot be obtained from this technique, because it only measured the relative frequency change. However, this is only beneficial for the present study, as we are only interested in changes of resistivity in a magnetic field and are not sensitive to static resistivity background.

As expected, due to an increase of spin disorder and phonon scattering as temperature decreases, the resistivity sharply decreases below T_N. The reconstructed resistivity (solid line) is compared to direct four-point measurements performed on the sample from the same batch. Evidently, the quantitative agreement is good. Similarly, a good agreement was obtained for $\rho(T)$ measured in various applied magnetic fields where the magnetoresistance followed a Kohler rule as described in detail in Ref. 12.
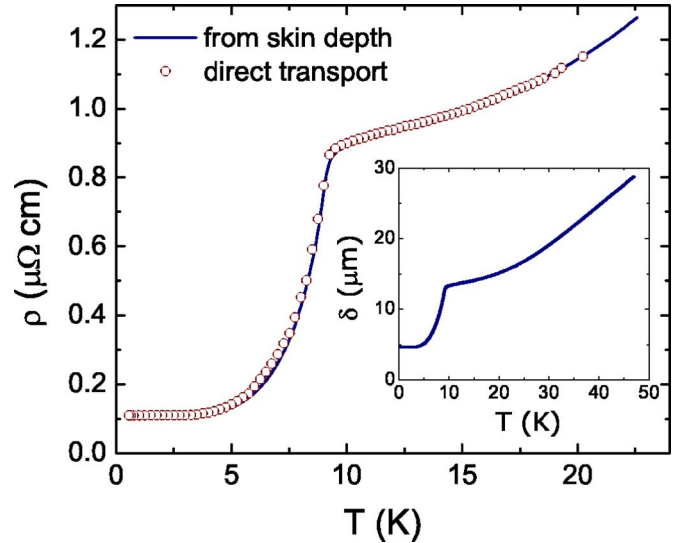

FIG. 2. (Color online) Resistivity versus temperature for $SmAgSb_2$ single crystal measured directly (open symbols) and inferred from the skin depth measurements (solid line). The inset shows variation of the skin depth with temperature.

The oscillations of resistivity were obtained from the measured oscillations in the skin depth, which in turn were obtained from the oscillating frequency shift. An example of the raw data for both, $CeAgSb_2$ and $SmAgSb_2$ are shown in Fig. 3 in the top and bottom panels, respectively.

For $SmAgSb_2$ the resistivity oscillations reconstructed from the frequency shift are shown as a function of H^{-1} in Fig. 4. A smooth $\rho(H)$ background was subtracted using nonoscillating piecewise cubic Hermite interpolating polynomial algorithm in MATLAB.

Power spectra were obtained from the oscillations by using a fast Fourier transformation (FFT). The result is shown in Fig. 5. At a first glance, the spectra are quite similar to
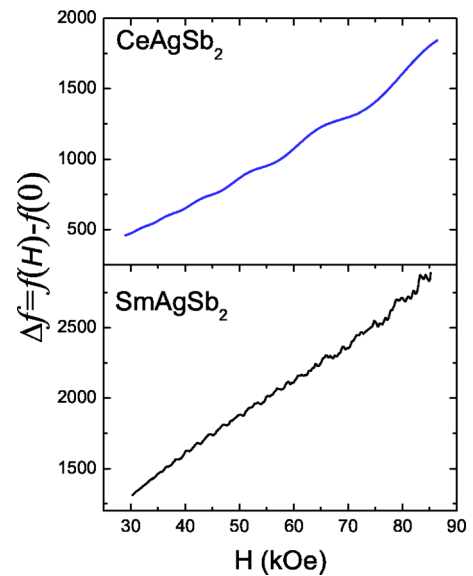

FIG. 3. (Color online) Relative frequency shift in a magnetic field for $CeAgSb_2$ (top) and $SmAgSb_2$ (bottom) at 1.8 K.
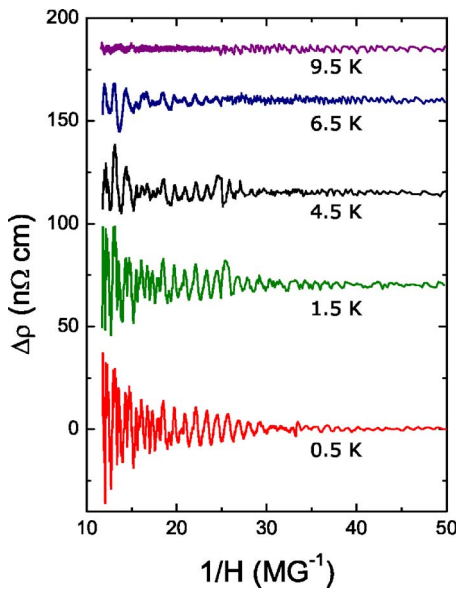
FIG. 4. (Color online) Oscillations of the reconstructed resistivity versus reciprocal magnetic field in SmAgSb$_2$ single crystal measured at several temperatures below T_c. The curves are offset for clarity.

those reported from the previous direct measurements of the SdH oscillations.[13] However, closer inspection reveals additional details, most likely due to higher sensitivity of our measurements.

Figure 6 shows low-frequency detailed spectrum of oscillations obtained at $T=0.5$ K. In addition to the previously observed main β peak, there is a sharp adjacent peak at 0.9 MG, which was apparently unresolved in previous direct measurements, at least down to 1.8 K. This new peak is not a secondary combination of α and β frequencies and we
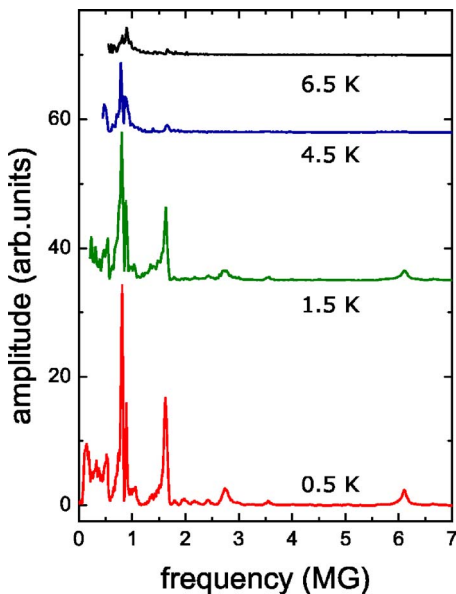

FIG. 5. (Color online) Power spectra of Shubnikov-de Haas oscillations obtained from the data shown in Fig. 4. The curves are offset for clarity.
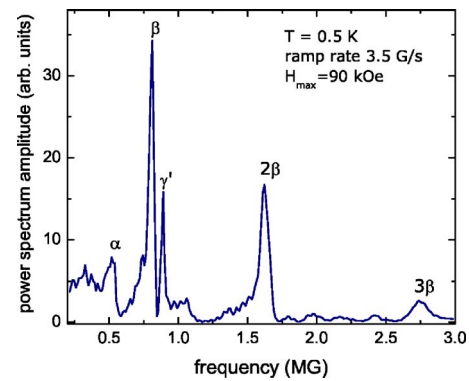

FIG. 6. (Color online) Low-frequency portion of the power spectra of Shubnikov-de Haas oscillations measured in SmAgSb$_2$ at $T=0.5$ K.

attribute it to the γ' orbit shown below in Fig. 11(a).

Since our measurements are quantitative, it is possible to plot temperature dependence of the observed peaks. Figure 7 demonstrates that these dependencies are quite different. Both peaks vanish as the Néel temperature is approached.

In principle, we cannot rule out the influence of de Haas-van Alphen oscillations of magnetization [via μ term in Eq. (5)], however, additional features observed in our data are not seen in the measured dHvA spectra and, conversely, we do not see the strongest peaks of the dHvA oscillations. Instead, we see all SdH peaks and resolve additional features. In addition, deep inside magnetically ordered state and in high fields μ is close to unity. The oscillatory part is a response to a very small excitation field superimposed on a very large DC field. To further explore applicability of the developed technique and rule out unexpected nonlinear or magnetic effects, we also measured CeAgSb$_2$, which is isostructural to SmAgSb$_2$, but showed a well-resolved, single frequency SdH oscillation of 0.25 MG (Ref. 13). Figure 8
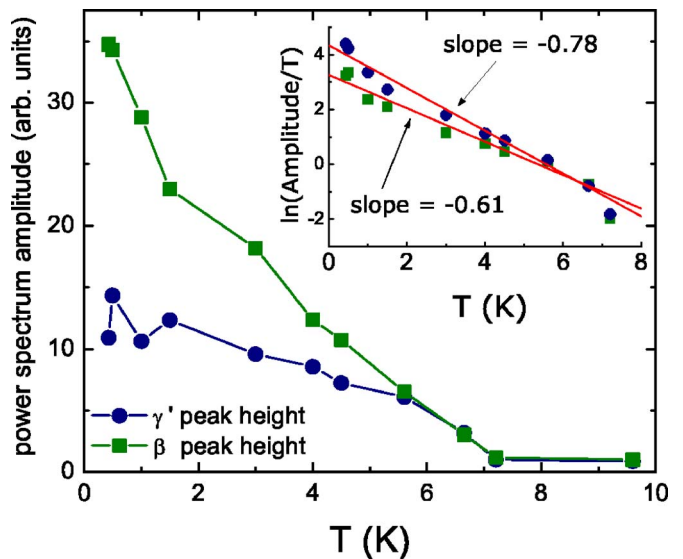

FIG. 7. (Color online) Temperature dependence of β and γ' peaks power spectrum amplitudes in SmAgSb$_2$. Inset: log of Fourier transform amplitude over T—used in calculation of the effective mass.
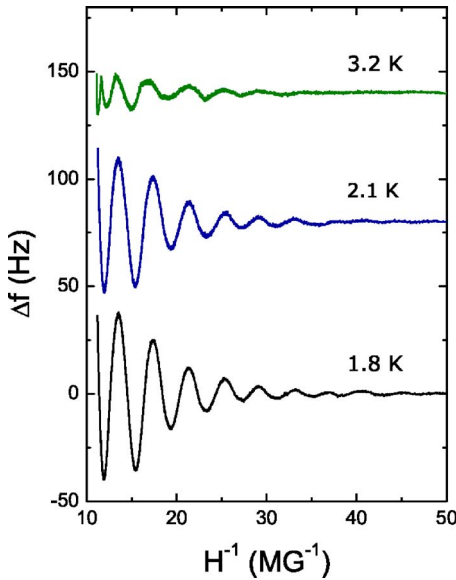
FIG. 8. (Color online) Shubnikov-de Haas oscillations (raw data in terms of the resonant frequency shift) in single crystal CeAgSb$_2$ measured at indicated temperatures. The curves are offset for clarity.

shows the result of our measurements at various temperatures below T_c. Clearly, we observe a single frequency oscillations at 0.25 MG.

A typical smallest oscillation amplitude of measured resonant frequency was about 20 Hz (Fig. 8) whereas our resolution is better than 0.1 Hz. We therefore are able to measure samples at least 10–100 times smaller than used here (depending on their resistivity and surface quality).

Figure 9 shows power spectra for the SdH oscillations, which is similar to these reported previously.[13,14] The amplitude of oscillations decreased with the increasing temperature much more rapidly compared to SmAgSb$_2$. This de-
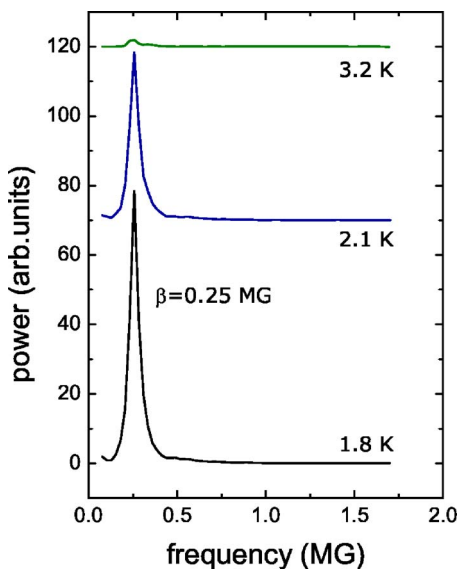

FIG. 9. (Color online) Power spectra of Shubnikov-de Haas oscillations observed in CeAgSb$_2$ single crystal. The curves are offset for clarity.

crease, however, is very similar to recent measurements of SdH effect in the same compound where signal vanishes just above 3 K.[14]

V. DISCUSSION

The difference in relative amplitudes between dHvA and SdH oscillations is not surprising and is determined by the effective mass via $\alpha_r/M_r \propto m_c^2$ [see Eqs. (1) and (3)]. The temperature dependence of the amplitude of the SdH oscillations in CeAgSb$_2$, taken for several single oscillations, Fig. 8, or FFT amplitude, Fig. 9, allows us to roughly estimate the effective mass associated with this orbit to be $m^* = 0.6 \pm 0.1 m_0$. From Fig. 7 an estimate of the effective mass of the new orbit in SmAgSb$_2$ below T_N, between 2 and 6 K, gives an approximate value of $0.27 m_0$, close to the effective mass, $0.21 m_0$, of the neighboring β orbit evaluated in a similar temperature/field range and to the value for a β orbit in LaAgSb$_2$.[13] This low value also explains the substantial difference between amplitudes of SdH and dHvA effects.

The results of electronic structure calculations of the two nonmagnetic (NM) compounds from the family RAgSb$_2$ where $R = Y$ and La were discussed previously by Myers *et al.*[13] It was assumed that substitution of Y or La for rare-earth element should not significantly change the electronic structure near the Fermi energy, E_F, because $4f$ electrons are strongly localized. Observation of additional frequencies in SmAgSb$_2$ was explained by the smaller residual resistivity and possible change of the Fermi surface produced by the new periodicity due to antiferromagnetic ordering.[13] In this paper we revisit that assumption and calculate the band structure specifically for the SmAgSb$_2$ using the tight-binding, linear muffin-tin orbital (TB-LMTO) method within the atomic sphere approximation (ASA).[16,17] The local density approximation parametrization due to von Barth and Hedin[18] of the spin-density functional has been used and the $4f$ states were treated as core states.

Since the spin structure in the AFM ordered state has not been experimentally determined, we assume the simplest configuration with magnetic moments of the two Sm^{3+} ions (in $4f^5$ configuration) in the unit cell pointing in the opposite directions. Such a configuration has an energy lower by $\Delta E = 84$ K/cell compared to the ferromagnetically ordered state. In order to estimate the Neél temperature, T_N, we can use the Heisenberg model. The T_N calculated in the mean-field approximation is equal to $\frac{2}{3}J_0$, where J_0 is the effective exchange parameter and it corresponds to the sum of the interactions of one magnetic moment with all others. Using the information about ΔE and the assumption that the only nonzero interaction corresponds to the nearest neighbors, we obtain the expression for $J_0 = \Delta E/4$. The estimated $T_N = 14$ K is in reasonable agreement with Neél temperature of 9.5 K observed in the compound.

Figure 10 shows the electronic structure of SmAgSb$_2$ along several high-symmetry directions. The assumed AFM ordering (bands shown by dashed lines) lifts the degeneracy in some symmetry directions. However, such modification of the electronic structure does occur for the bands crossing the Fermi level. Hence, almost all the difference between the
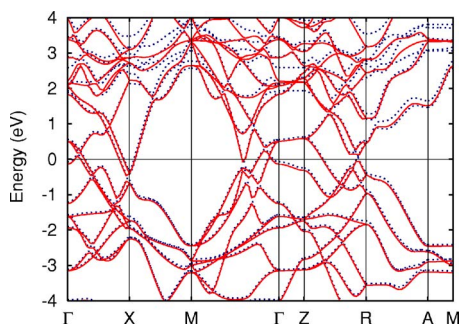
FIG. 10. (Color online) Band structure of SmAgSb$_2$ calculated from ASA TBLMTO. E_F corresponds to zero energy. The nonmagnetic result is shown by the solid lines; the antiferromagnetic case is shown by the dotted lines.

Fermi surfaces of antiferromagnetic SmAgSb$_2$ and nonmagnetic YAgSb$_2$ (Ref. 13) is a downshift of the Fermi level position compared to the band labeled "1" in Ref. 13. This shift of E_F leads to the modification of a nearly spherical FS sheet (band 1) centered at a Γ point, which is transformed into a torus as shown in Fig. 11(a) with frequency of 1 MG for $H\|c$ axis for the internal circle orbit γ', close to the frequency of 0.82 MG of an orbit labeled β in Fig. 6 of the second band.

Another FS sheet which changes significantly corresponds to band 2 and is shown in Fig. 11(b). Band 2 is also centered at a Γ point. In addition to a mostly cylindrical part with the axis along k_z as in YAgSb$_2$, eight pillow-shaped segments now appear around the main cylinder with the frequency of the δ'' orbit equal to 1.78 MG. We therefore conclude that previously unresolved peak (closest to β) in SmAgSb$_2$ is determined by the γ' orbit. The appearance of this orbit is caused by the shift of E_F position with respect to band 1 compared to YAgSb$_2$ where this orbit is absent. This shift is produced by filling $4f$ states in Sm^{3+} by five electrons that lead to a slight change of the d-band occupancy compared to Y-based compound. Additional support to our assignment of the observed new peak to a γ' orbit comes from the fact that this frequency was not observed when a magnetic field was oriented perpendicular to the c axis.

In conclusion, a high resolution method for contactless measurements of the resistivity via normal skin depth was developed to probe Shubnikov-de Haas oscillations in small metallic samples. Torque measurements can be used to ob-
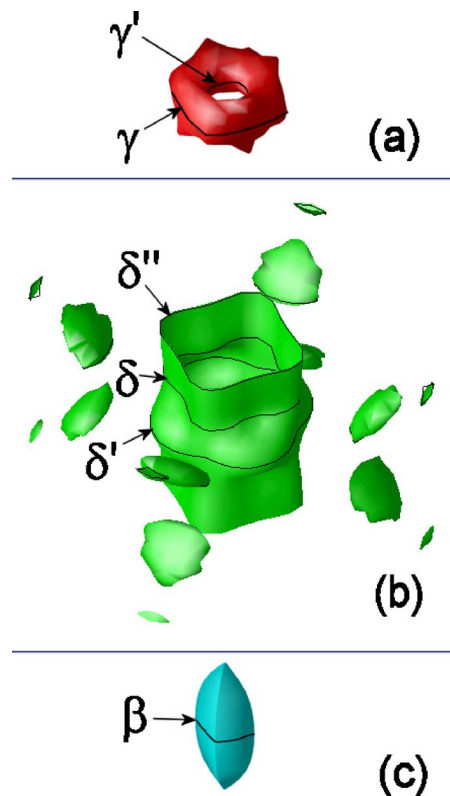

FIG. 11. (Color online) Fermi surface of SmAgSb$_2$ corresponding to (a) band 1, (b) band 2, and (c) band 3. The extremal orbits indicated by greek letters and shown by arrows.

tain de Haas-van Alphen oscillations and presented technique can be applied to the same small samples to obtain Shubnikov-de Haas signal without modifying the samples (to attach contacts). The application of the method was demonstrated on a RAgSb$_2$ system. Fine details of the oscillation spectrum (a new γ' orbit) was resolved experimentally and explained with refined bandstructure calculations.

*Electronic address: prozorov@ameslab.gov

[1] D. Shoenberg, *Magnetic Oscillations in Metals* (Cambridge University Press, Cambridge, 1984).

[2] M. V. Kartsovnik, Chem. Rev. (Washington, D.C.) **104**, 5737 (2004).

[3] J. D. Jackson, *Classical Electrodynamics* (John Wiley & Sons, Inc., New York, 1998), p. 220.

[4] A. B. Pippard, Philos. Trans. R. Soc. London, Ser. A **250**, 325 (1957).

[5] R. Prozorov, R. W. Giannetta, A. Carrington, and F. M. Araujo-Moreira, Phys. Rev. B **62**, 115 (2000).

[6] R. Prozorov, R. W. Giannetta, A. Carrington, P. Fournier, R. L. Greene, P. Guptasarma, D. G. Hinks, and A. R. Banks, Appl. Phys. Lett. **77**, 4202 (2000).

[7] E. S. Choi, E. Jobilong, A. Wade, E. Goetz, J. S. Brooks, J. Yamada, T. Mizutani, T. Kinoshita, and M. Tokumoto, Phys. Rev. B **67**, 174511 (2003).

[8] T. Coffey, Z. Bayindir, J. F. DeCarolis, M. Bennett, G. Esper, and

C. C. Agosta, Rev. Sci. Instrum. **71**, 4600 (2000).

[9] J. R. Cooper, Phys. Rev. B **54**, R3753 (1996).

[10] M. Brylak, M. H. Moeller, and W. Jeitschko, J. Solid State Chem. **115**, 305 (1995).

[11] O. Sologub, H. Noeel, A. Leithe-Jasper, P. Rogl, and O. I. Bodak, J. Solid State Chem. **115**, 441 (1995).

[12] K. D. Myers, S. L. Bud'ko, I. R. Fisher, Z. Islam, H. Kleinke, A. H. Lacerda, and P. C. Canfield, J. Magn. Magn. Mater. **205**, 27 (1999).

[13] K. D. Myers, S. L. Bud'ko, V. P. Antropov, B. N. Harmon, P. C. Canfield, and A. H. Lacerda, Phys. Rev. B **60**, 13371 (1999).

[14] E. Jobiliong, J. S. Brooks, E. S. Choi, H. Lee, and Z. Fisk, Phys. Rev. B **72**, 104428 (2005).

[15] P. C. Canfield and Z. Fisk, Philos. Mag. B **65**, 1117 (1992).

[16] O. K. Andersen, Phys. Rev. B **12**, 3060 (1975).

[17] O. K. Andersen and O. Jepsen, Phys. Rev. Lett. **53**, 2571 (1984).

[18] U. von Barth and L. Hedin, J. Phys. C **5**, 1629 (1972).